Measurement of the $B(E2\uparrow)$ strengths of ^{36}Ca and ^{38}Ca

N. Dronchi,[1,*] D. Weisshaar,[2] B. A. Brown,[2,3] A. Gade,[2,3] R. J. Charity,[4] L. G. Sobotka,[1,4] K. W. Brown,[2,5] W. Reviol,[6] D. Bazin,[2,3] P. J. Farris,[2,3] A. M. Hill,[2,3] J. Li,[2] B. Longfellow,[2,3] D. Rhodes,[2,3] S. N. Paneru,[2] S. A. Gillespie,[2] A. Anthony,[2] E. Rubino,[2] and S. Biswas[2]

[1]*Department of Physics, Washington University, St. Louis, Missouri 63130, USA*
[2]*Facility for Rare Isotope Beams, Michigan State University, East Lansing, Michigan 48824, USA*
[3]*Department of Physics and Astronomy, Michigan State University, East Lansing, Michigan 48824, USA*
[4]*Department of Chemistry, Washington University, St. Louis, Missouri 63130, USA*
[5]*Department of Chemistry, Michigan State University, East Lansing, Michigan 48824, USA*
[6]*Physics Division, Argonne National Laboratory, Argonne, Illinois 60439, USA*

(Received 20 December 2022; accepted 28 February 2023; published 14 March 2023)

The $B(E2,\, 0_1^+ \rightarrow 2_1^+)$ strengths of ^{36}Ca and ^{38}Ca are measured to be 131(20) e^2fm^4 and 101(11) e^2fm^4, respectively. The $B(E2)$ value for ^{36}Ca required a measurement of the p/γ branching ratio because the 2^+ state is proton unbound. This branching ratio is $B_p = 0.087(8)$. These $B(E2)$ and branching-ratio values can be reproduced in the shell-model with the ZMB2 interaction, an interaction that predicts the $Z = 20$ sd-shell closure is incomplete with large proton pf-shell occupancies in the ground state. These occupancies are at odds with other shell-model and energy-density-functional calculations of ^{36}Ca. New data are used to provide an update on constraints of the density dependence of the symmetry energy through mirror charge-radii differences as well as to help reduce uncertainties of the astrophysical important ^{35}K(p,γ) reaction.

DOI: 10.1103/PhysRevC.107.034306

I. INTRODUCTION

The reduced electric quadrupole matrix element or $B(E2)$ strength between the 0^+ ground state and the first 2^+ excited state in even-even nuclei is an important quantity that provides information on nuclear structure. This probe of nuclear structure can provide information on the degree of collectivity of the ground state as one moves across the chart of nuclides towards the drip line. The $B(E2)$ strength is also intrinsically linked to the γ-ray partial width that, when combined with the proton partial width, can be used in astrophysical capture reaction rates.

Trends in the $B(E2)$ values across an isotopic or isotonic chain have been used to probe the breakdown of magic numbers. As one removes protons from ^{40}Ca, the $N = 20$ magic number is known to disappear at ^{32}Mg, the center of a so-called "island of inversion". Here, neutron intruder pf-shell orbitals are strongly occupied in the ground state (see Ref. [1] and references within). The mirror of ^{32}Mg would be ^{32}Ca which is well beyond the proton drip line and difficult to explore. Currently, ^{36,38}Ca are the lightest even-even Ca isotopes that can provide crucial evidence for the evolution of the $Z = 20$ shell towards the proton drip line through measured $B(E2)$ strengths.

In explaining the nuclear charge radii of calcium isotopes within the shell model, Caurier *et al.* [2] argued that even near ^{40}Ca, the $Z = 20$ and $N = 20$ shell closures were weakened with substantial occupancy of both neutron and proton pf shells in the ground state. The interaction obtained, later referred to as ZBM2, has been used to calculate charge radii, for both ground and isomeric states, and to compare to the available data in this mass region [3,4]. Other recent studies have employed shell-model interactions which predict very little proton pf occupancy in the ground state. One example is the work of Lalanne *et al.* [5] in which an estimated $B(E2)$ value is used for ^{36}Ca to evaluate the ^{35}K$(p,\gamma)^{36}$Ca reaction rate, a rate of significance for type I x-ray burst calculations.

The recent measurement of the charge radii of ^{36,38}Ca were interpreted with nuclear density functional theory by Miller *et al.* [6]. They indicate that the charge radius is strongly impacted by nuclear superfluidity and the weakly bound nature of the protons. For ^{36}Ca, the proton $f_{7/2}$ level was predicted to be located above the Coulomb barrier, indicating properties of this nuclei would be strongly affected by the proton continuum. In these calculations the proton pf-shell occupancy for ^{36}Ca$_{\text{g.s.}}$ is only about 13%.

To the extent that the $Z = 20$ shell closure is complete, the $B(E2)$ strengths for ^{36,38}Ca should be very small as both excitations of the 2^+ states from their ground states is achieved only via neutron excitations. Any ground-state proton pf occupancy would greatly inflate the $B(E2)$ value and thus this quantity is very sensitive to the extent of the $Z = 20$ shell closure.

This work reports the previously unmeasured $B(E2,\, 0_1^+ \rightarrow 2_1^+)$ strength for ^{36}Ca. The determination of this reduced matrix element requires two separate measurements because the 2^+ state is unbound. We first performed a measurement of

*n.dronchi@wustl.edu

de-excitation γ rays following intermediate-energy Coulomb excitation, a method widely used in the study of nuclei far from stability [7]. To account for the competing proton decay branch, and thus to deduce the total Coulomb-excitation cross section, a second measurement was performed to determine the relative proton-to-γ decay widths. The present work also confirms the $B(E2)$ for ^{38}Ca measured by Cottle *et al.* [8] with improved precision. No proton-decay measurement is required in this case as the 2^+ state in ^{38}Ca is below the proton decay threshold.

An additional motivation for the measurement of the $B(E2)$ strength of ^{36}Ca comes from the proposal of Brown to use the difference in a mirror pair's rms charge radii to determine L, the density dependence of the symmetry energy [9,10]. In order to deduce L, it is essential to correct for any difference in the deformations of the mirror pair due to the calculations being based on a spherical model space [11]. The $B(E2)$ strength is a metric linked to collectivity and deformation of the nucleus. The inferred deformation can be used to correct the rms charge radii of mirror pairs for any such collectivity difference. To perform this correction, the rms charge radii and the $B(E2)$ values for both members of the pair must be known. With the recent hyperfine spectrum measurements by Miller *et al.* [6] that deduced the rms charge radius of ^{36}Ca, only the $B(E2)$ for ^{36}Ca remained undetermined to employ this logic for the ^{36}Ca - ^{36}S pair.

The γ-ray and proton partial widths (measured through the $B(E2)$ strength and branching ratio) also impact the rp process through the $^{35}\mathrm{K}(p,\gamma)^{36}\mathrm{Ca}$ reaction rate. The proton branch returns flux to ^{35}K, and to the $^{34}\mathrm{Ar}(p,\gamma)^{35}\mathrm{K}$ - $^{35}\mathrm{K}(\gamma,p)^{34}\mathrm{Ar}$ equilibrium. The (p,γ)-(γ,p) equilibrium is escaped through resonance capture to the 2^+ state in ^{36}Ca and, via the γ branch and subsequent β decay, populates ^{36}K.

Simulations of the rp process determined that the $^{35}\mathrm{K}(p,\gamma)^{36}\mathrm{Ca}$ reaction can be an important component to the shape of x-ray-burst light curves [12]. This reaction is dominated by resonant capture through the 2^+ state in ^{36}Ca and the predicted light curves were found to be sensitive to large changes in this resonance capture rate. This is a case where reducing the nuclear data uncertainties impacts the interpretation of expected astrophysical observations.

II. EXPERIMENTAL METHODS

In this paper, a pair of experiments for ^{36,38}Ca will be discussed. The first experiment, discussed in Sec. II A, measured the cross sections for γ decay following Coulomb excitation of ^{36,38}Ca beams. The second experiment, discussed in Sec. II B, measured the p/γ branching ratio of the 2^+ state in ^{36}Ca.

A. Coulomb excitation of ^{38,36}Ca with γ-ray spectroscopy

Intermediate-energy Coulomb excitation of the projectile is widely used to assess the low-lying states with quadrupole or octupole collectivity in rare isotopes that are available as beams of fast ions. The short interaction time at intermediate beam energies strongly favors single-step Coulomb excitation, providing selective access to typically $B(E2; 0_1^+ \to 2_n^+)$ and sometimes $B(E3; 0_1^+ \to 3_m^-)$ values in even-even nuclei. Within this experimental scheme, rare isotopes at velocities exceeding 30% of the speed of light are scattered off stable high-Z targets and are detected in coincidence with the de-excitation γ rays that tag and quantify the inelastic process [7,13]. While beam energies below the Coulomb barrier prevent nuclear contributions to the excitation process, peripheral collisions must be selected in the regime of intermediate-energy Coulomb scattering to exclude nuclear contributions. This is accomplished by restricting the analysis to events scattered at the most forward angles, corresponding to large minimum impact parameters in the collision [7].

A choice of impact parameters where "touching sphere + 2 fm" is exceeded has been shown to be sufficient to minimize nuclear contributions [14,15]. Angle-integrated Coulomb excitation cross sections are then translated into $B(E2)$ values using the Alder-Winther model of intermediate-energy Coulomb excitation [16].

The two rare-isotope beams containing ^{38}Ca (69.1 MeV/nucleon) and ^{36}Ca (76.9 MeV/nucleon) were produced from the fragmentation of a 140-MeV/nucleon ^{40}Ca primary beam delivered by the Coupled Cyclotron Facility at the National Superconducting Cyclotron Laboratory [17] impinging upon an 800-mg/cm^2 thick ^{9}Be production target and separated using a 300-mg/cm^2 Al wedge degrader in the A1900 fragment separator [18]. Both secondary-beam settings were optimized for purity, achieving ^{38}Ca and ^{36}Ca content purities of 85% and 11%, respectively. In the second case, ^{34}Ar was the most abundant contaminant. The projectile beams were scattered off a 257-mg/cm^2-thick Au foil located at the target position of the S800 spectrograph [19] and surrounded by the γ-ray tracking array GRETINA [20]. GRETINA consisted of 12 modules, housing four HPGe crystals each, with eight modules arranged at 90° and four modules at 58° with respect to the beam direction. The event-by-event Doppler correction was performed with respect to the spatial coordinates of the main interaction as deduced from online signal decomposition. GRETINA was treated as 48 independent crystals to minimize systematic uncertainties in the γ-ray detection efficiency [21]. The inelastic excitations of the projectile and target nuclei were quantified via the detection of the prompt de-excitation γ rays in GRETINA. The scattered projectiles were identified event-by-event using the S800 focal-plane detection system [22] together with a time-of-flight measurement. Position measurements in the S800 focal plane and ray tracing were used to determine the projectile's scattering angle on an event-by-event basis which is then gated on to limit the impact parameter of the collision. We followed the prescription developed in Ref. [23] to minimize the impact of the beam's angular emittance by choosing a slightly more conservative, i.e., smaller, maximum scattering angle as illustrated in Fig. 3 of [23].

B. Branching-ratio setup

The second experiment, also performed at the National Superconducting Cyclotron Laboratory, was set up to be sensitive to both γ- and proton-decay branches. A primary 140-MeV/nucleon ^{40}Ca beam impinged on a Be target to

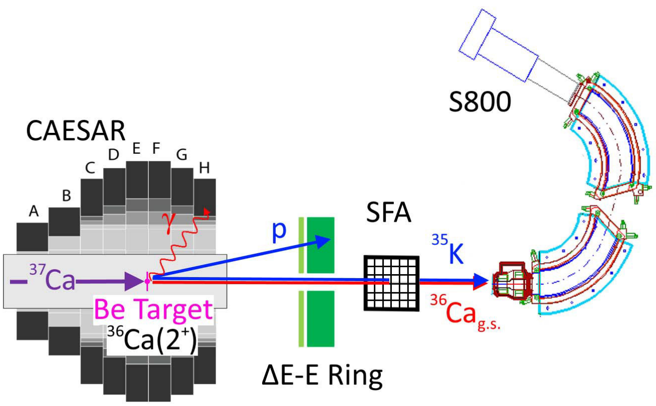

FIG. 1. Schematic of the experimental apparatus. The beam direction is from left to right. For the γ-ray emission from the 2^+ state, CAESAR detects the γ rays while the S800 identifies the ^{36}Ca residue. The proton is detected and identified in the ΔE-E [Si-CsI(Tl)] telescope ring array. The smaller angles of the ^{35}K and ^{36}Ca residues are measured by the scintillating fiber array (SFA) and the particle-identification and momentum of these fragments are measured with the S800 spectrograph.

remove three neutrons to produce a ^{37}Ca secondary beam. This secondary beam at 75 MeV/nucleon impinged on a 0.5-mm-thick Be target. The subsequent knock out of one more neutron populated states of ^{36}Ca, including the ground and 2^+ states of interest [24].

At the site of the ^{36}Ca production, we employed the combination of detectors diagrammed in Fig. 1. The photon detector is the CAESium-iodide scintillator ARray (CAESAR) [25] which is centered around the Be target. CAESAR was arranged in eight rings with a total of 163 working scintillators spanning 55° to 163°. The two most upstream rings, labeled A and B, consisted of 3 in. × 3 in. × 3 in. CsI(Na) crystals while the other six rings, labeled C-H, were 2 in. × 2 in. × 4 in. crystals. CAESAR has a high full-energy-peak efficiency for detecting the 3-MeV γ rays of interest of ≈15% with the trade off (relative to GRETINA from Sec. II A) of only modest energy resolution, ≈8% FWHM.

For the proton-decay branch, the excitation spectrum of ^{36}Ca was determined using the invariant-mass method [26]. Protons were detected using a ΔE-E [Si-CsI(Tl)] telescope ring array. This array consists of a 1-mm-thick S4 double-sided silicon strip detector (DSSD), manufactured by Micron Semiconductor, backed by an annular array of CsI(Tl) detectors. The DSSD is wired into 128 concentric rings and 128 annular sectors. The CsI(Tl) crystals were arranged directly behind the S4 detector in two concentric rings of four (inner) and 16 (outer) crystals. This telescope provides particle identification as well as the momentum vector for the protons coming from the decay of the ^{36}Ca(2^+) state.

The nuclei of interest, ^{35}K and ^{36}Ca (the former after proton emission), pass through a scintillating-fiber array (SFA) made of an orthogonal pair of scintillating fiber ribbons. Each ribbon consists of 64 fibers of square (250 μm × 250 μm) cross section. This array records precise angular information for the heavy residue. The residues then enter the S800 spectrograph where two rigidity settings were used, one tuned for the best acceptance of ^{36}Ca while blocking some ^{37}Ca beam particles ($B\rho = 1.9696$ Tm) and the second tuned for the best ^{35}K acceptance ($B\rho = 2.0468$ Tm).

TABLE I. Cross sections and $B(E2\uparrow)$ values for the projectile (p) and target (Au) excitations. The cross sections are integrated from 0 to a maximum scattering angle of $\theta_{\rm max}^{\rm lab} = 55$ mrad for the ^{38}Ca, ^{36}Ca, ^{34}Ar, and ^{37}K projectiles at 62.6, 70.5, 64.3, and 59.8 MeV/nucleon midtarget beam energies, respectively. The cross section for the excitation of the proton-unbound 2_1^+ state in ^{36}Ca was corrected for the proton branch reported in this work. The $B(E2\uparrow)$ for the beam contaminant ^{34}Ar was determined as well and found to agree with the literature value of 220(30) e^2fm^4 [34] within 2σ.

proj	$E(2_1^+)$ (keV)	σ_I^p (mb)	$B(E2\uparrow;\text{proj})$ (e^2fm^4)	$\sigma_I^{\rm Au}$ (mb)	$B(E2\uparrow;\text{Au})$ (e^2fm^4)
^{38}Ca	2213(2)	17.5(19)	101(11)	49.5(18)	4570(170)
^{36}Ca	3049(3)	22.4(34)	131(20)	52.8(30)	4820(280)
^{34}Ar	2091(2)	52.1(29)	293(16)	44.2(16)	4960(180)
^{37}K	-	-	-	45.2(32)	4620(330)

CAESAR was energy calibrated using several standard γ-ray sources and an AmBe source for a 4.44-MeV calibration point. For the ΔE-E ring telescope, a proton beam with a 0.5% $\Delta p/p$ acceptance was degraded with 1.0[8.6]-mm-thick Be[Al] target to get CsI(Tl) calibration points at 75.2[58.8] MeV. A mixed α source was used to calibrate the DSSD.

III. EXPERIMENTAL RESULTS

A. Measurement of the $B(E2)$ strength

The maximum scattering angle of $\theta_{\rm max}^{\rm lab} = 55$ mrad was chosen for all projectiles in the present work to extract angle-integrated cross sections $\sigma_I = \sigma(\theta \leqslant \theta_{\rm max})$ from the number of efficiency-corrected γ rays relative to the number of incoming projectiles and number density of target nuclei. For this, the simulation tool UCGretina [27] was utilized to determine the effects of the Lorentz boost, target absorption, and angular distribution in order to rescale the measured efficiency curve for GRETINA to an in-beam efficiency. The angular distribution coefficients were obtained using the excitation amplitudes from the Alder-Winther model of intermediate-energy Coulomb excitation [16].

As test cases, the $B(E2; 3/2_1^+ \rightarrow 7/2_1^+)$ transition strength from the ground to the 547.5 keV excited state in the Au target was analyzed for various incoming isotopes in the secondary beam settings. The γ-ray peak for the target excitation is not impacted by the Doppler effect and its intensity can be cleanly extracted from the laboratory-frame γ-ray spectrum. The 5 × 5 cm Au target caused an estimated 10% detection efficiency loss due to absorption of the 547.5 keV γ rays emitted at 90° and traversing the foil. The effect of the γ-ray angular distribution with preferential emission towards 90° is of equal magnitude. The extracted $B(E2\uparrow;\text{Au})$ values are listed in Table I and are in agreement with the adopted value of 4500(400) e^2fm^4 [28].

γ rays from the de-excitations of the projectile were detected and the energies Doppler corrected for ^{36,38}Ca (see

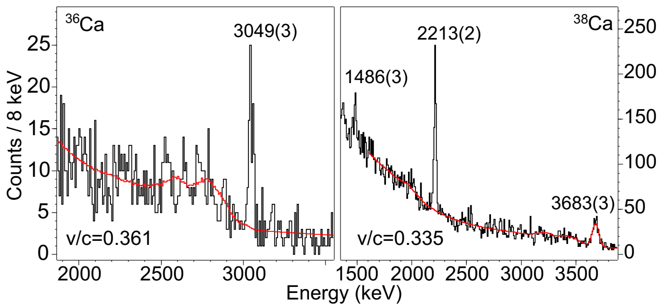

FIG. 2. Doppler reconstructed γ-ray spectra showing the de-excitation of the populated levels in ^{36}Ca (left) and ^{38}Ca (right). The fit modeling the background contributions to the 2_1^+ states are used to extract the intensity by integration is superimposed (red).

Fig. 2) and ^{34}Ar (not shown). Only the known $2_1^+ \rightarrow 0_1^+$ transition [24,29] was observed to decay through γ-ray emission for ^{36}Ca with the level scheme shown in Fig. 3. The $2_1^+ \rightarrow 0_1^+$ transition, as well as two additional transitions both previously reported by Cottle *et al.* [8], are observed for ^{38}Ca. Relevant levels for ^{38}Ca are included in Fig. 3 and are found to be consistent with the level scheme presented in Ref. [30], with the peak at 3683(3) keV corresponding to the $2_2^+ \rightarrow 0_1^+$ transition and the 1486 keV peak predominantly due to the $3_1^- \rightarrow 2_1^+$ decay with a small contribution from the 1471 keV $2_2^+ \rightarrow 2_1^+$ transition impossible to exclude. Peak areas were determined by integration following the precise modeling of the background that is composed of the Compton continua, simulated with UCGretina, on top of a two-component exponential background.

Table I presents the cross section and $B(E2;\uparrow)$ values for the excitation of the first 2^+ state in ^{36,38}Ca and ^{34}Ar. The reported values are derived from the efficiency-corrected peak area and, in the case of ^{36}Ca corrected for the proton branch. No feeding corrections are needed for ^{36}Ca. The determination of $\sigma_I^p(2_1^+)$ for ^{38}Ca, the feeding from the 1486(3) keV transition was subtracted. The resulting $B(E2\uparrow)$ value of 101(11) e^2fm^4 is in good agreement with the previously reported value of 96(21) e^2fm^4 [8], however, the present value has a significantly improved precision.

Neglecting a possible branch to the 2_1^+ state, the cross section and $B(E2\uparrow)$ value are $\sigma_I^p(2_2^+) = 16.0(15)$ mb and $B(E2\uparrow; {}^{38}\text{Ca}(2_2^+)) = 108(10)$ e^2fm^4. However, if there was no $2_2^+ \rightarrow 2_1^+$ branch then the 1486 keV peak would correspond entirely to the $3^- \rightarrow 2^+$ transition. The yield of this transition would then imply a $B(E3)$ value of 78(21) W.u. for $3_1^- \rightarrow 0_1^+$ decay. This exhausts the recommended upper limit of 50 W.u. [33] for such a transition and exceeds the corresponding value in the mirror nucleus by a factor of 4. While this puzzle does not impact the extraction of the $B(E2)$ value for the excitation of the first 2^+ state, it is an interesting challenge that requires the precise measurement of the 2_2^+ branching ratios. We note that the $3_1^- \rightarrow 0_1^+$ branch was limited recently to less than 1% relative to the $3_1^- \rightarrow 2_1^+$ transition [30].

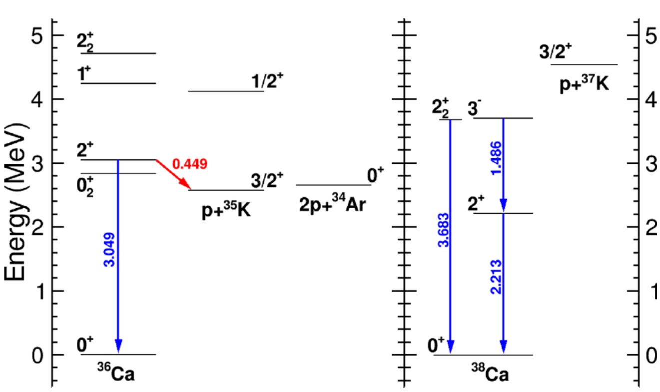

FIG. 3. Level schemes for ^{36}Ca (left) and ^{38}Ca (right) showing levels relevant to this paper. The one- and two-proton separation energies for ^{36}Ca are adapted from Ref. [31] with levels taken from Ref. [32]. Levels for ^{38}Ca and their decays are adapted from Ref. [30].

B. Measurement of proton branching ratio

γ rays detected by CAESAR gated on a ^{36}Ca residue recorded in the S800 provide the number of ^{36}Ca $+\gamma$ events. Protons detected in the ΔE-E ring telescope in coincidence with ^{35}K residues are used for the invariant-mass reconstruction. These two quantities constitute the branching ratio measurement as

$$B_p = \frac{N_{\text{events}}(^{35}\text{K} + p)}{N_{\text{events}}(^{36}\text{Ca} + \gamma) + N_{\text{events}}(^{35}\text{K} + p)}. \tag{1}$$

To relate the quantities in this equation to experimental observables, we define N_p and N_γ as the number of detected proton and γ-ray decays, and ε_γ as CAESAR's γ-ray efficiency, ε_p for the ΔE-E ring-telescope efficiency for protons, and $\varepsilon_{35K}/\varepsilon_{36Ca}$ for a relative S800 and SFA efficiency for the two residues. A beam intensity I_p or I_γ is required to normalize the counts from the different S800 settings required for the two decay paths. Employing these efficiencies, the branching ratio is

$$B_p = \frac{N_p/\varepsilon_p}{\left(\frac{N_\gamma}{\varepsilon_\gamma}\right)\left(\frac{\varepsilon_{35\text{K}}}{\varepsilon_{36\text{Ca}}}\right)\left(\frac{I_p}{I_\gamma}\right) + \frac{N_p}{\varepsilon_p}}. \tag{2}$$

1. γ branch

The CAESAR γ-ray energy spectrum recorded in coincidence with ^{36}Ca is plotted in Fig. 4. Each event was Doppler corrected based on the measured velocity of the ^{36}Ca residue and reconstructed with an angle based on the center of the CAESAR crystal that registered the highest energy deposition. No add-back between neighboring detectors was applied.

For an estimate of the background, the ^{35}K + γ channel was employed as only ^{35}K(g.s.) is particle-bound with no excited states that decay through γ-ray emission. All detected γ rays in coincidence with ^{35}K must be from background processes. This background was incorporated into the fit shown in Fig. 4 in three ways: by fitting a double exponential to this background data, by applying a smoothing function to this background data, or by scaling the contribution based on the ratio of ^{35}K to ^{36}Ca residues detected in the S800. The last of

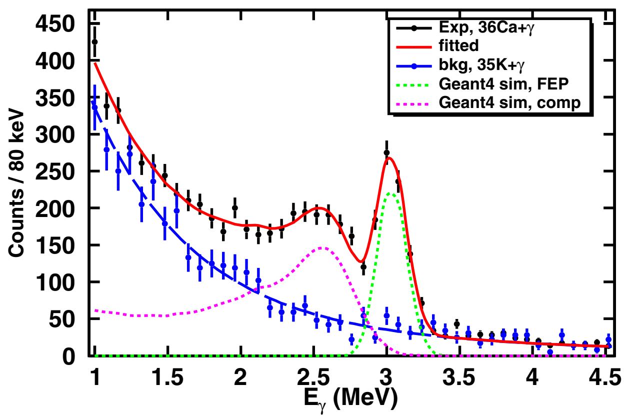

FIG. 4. Fit of the γ-ray energy spectrum in coincidence with identified ^{36}Ca residues. The shape of the background component (blue curve) is taken as a double exponential fit to the blue data points from $^{35}\mathrm{K}+\gamma$ events. The full-energy peak (green curve) and Compton-scattering and pair production components (magenta curve) were obtained from GEANT4/UCCAESAR simulations. The magnitudes of all three components were varied in the fit with the scaling of the FEP giving $N_\gamma/\varepsilon_\gamma$.

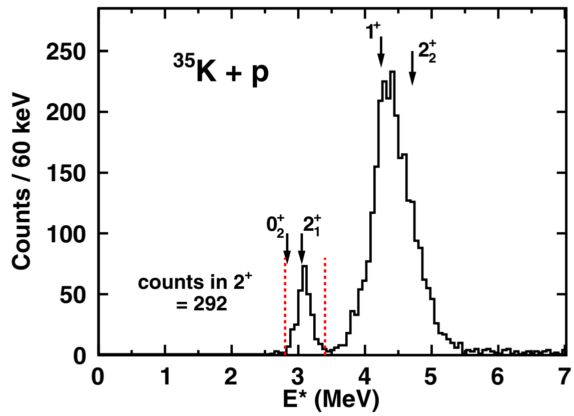

FIG. 5. Excitation energy spectrum of $^{36}\mathrm{Ca} \to {}^{35}\mathrm{K}+p$ decay obtained with the invariant-mass method. The 2^+ state is centered around 3-MeV excitation energy with red-dotted lines indicating the upper and lower limits of the energy gate. There is also a large population of the 1^+ state which was identified by Lalanne *et al.* [5].

which yielded an efficiency that was consistently between the other two and within the systematic error reported.

UCCAESAR [35,36], a simulation code built on the GEANT4 [37] toolkit, was used to handle the detector efficiency and response. The efficiency was used to convert the number of detected γ-ray events into the number of $^{36}\mathrm{Ca}(2^+)$ events that decayed through γ-ray emission, $N_\gamma/\varepsilon_\gamma$. The detector response was split into the full-energy-peak (FEP) detection and Compton-scattered or escape peaks (comp).

Through multiple fits, it was determined that $N_\gamma/\varepsilon_\gamma = 7800 \pm 356(\mathrm{stat}) \pm 470(\mathrm{syst})$. The origin of the systematic uncertainty comes from the different methods used to fit the simulation of the 3.049-MeV γ ray. First, the plot was fitted with a double exponential describing the background where the detector resolution was varied as well as the range of the fit. Varying the resolution and range of the fit both gave values within the average statistical uncertainty and resulted in a value of $N_\gamma/\varepsilon_\gamma = 8063 \pm 309(\mathrm{stat})$. This process was repeated with the same background, except a smoothing function was applied before fitting, resulting in a lower value $N_\gamma/\varepsilon_\gamma = 7539 \pm 355(\mathrm{stat})$. This higher statistical uncertainty was chosen for the overall statistical uncertainty.

For the systematic uncertainty, the highest and lowest value from all of these fits gives the range of N_γ, where the range/2 is used for a systematic uncertainty. The systematic uncertainty was calculated to be $\delta(N_\gamma/\varepsilon_\gamma)(\mathrm{syst}) = 470$.

2. Proton branch and detection efficiencies

The ^{36}Ca excitation spectrum obtained with the invariant-mass method is shown in Fig. 5 where the gate used to select the events from the decay of the 2^+ state is indicated by the two vertical red-dotted lines.

The 2^+ peak in ^{36}Ca lies in a region of the experimental spectrum with virtually no background and thus the peak can be directly integrated to find the number of detected proton decays, $N_p = 292 \pm 17(\mathrm{stat})$. There is a question on possible contributions from the decay of the 0_2^+ state which is expected to have a similar excitation energy as the 2_1^+ state. The recent measurement of Lalanne *et al.* [32] found the 0_2^+ state lies 230(13) keV below the 2_1^+ state [32] and was isolated by gating on a ^{36}Ca fragment in their zero-degree detector. This suggests that if the 0_2^+ state proton decays, it would have a long lifetime. The excited residue would travel a substantial distance before decay and miss our charged particle telescope. Indeed with its lower excitation energy, the d-wave partial proton decay width of this state is heavily retarded. Single-particle estimates with the quoted level energy are $\approx 10^{-9}$ eV suggesting that we should not have observed any contributions from this state in our invariant-mass spectrum. Additionally, we do not expect the 0_2^+ state to be significantly populated as the spectroscopic factors for neutron knockout from ^{37}Ca to the 2_1^+ and 0_2^+ states are 0.42 and 0.02, respectively (ZBM2 interaction).

The proton detection efficiency was simulated with the S800 acceptance, using Monte Carlo simulations taking into account the geometry as well as other constraints [26]. The simulation resulted in a detection efficiency of $\varepsilon_p = 0.764(5)$.

There is a gap in the ring telescope between the inner and outer rings of CsI(Tl) crystals where protons can pass through the inner ring and either stop in the wrapping material of the crystals or cross into the outer ring of crystals. This leads to a loss of proton identification efficiency. The magnitude of this loss was determined using singly detected protons with kinetic energy in the same range as those associated with the decay of the 2^+ state. The yield of these identified protons, shown in Fig. 6, varies smoothly as a function of the ring number of the S4 silicon detector except for ring numbers from 45 to 55 where a dip in the yield from this effect is observed. A correction to the proton detection efficiency for these rings is determined from the reduction relative to a linear interpolation based on the neighboring strips (shown by the red line in

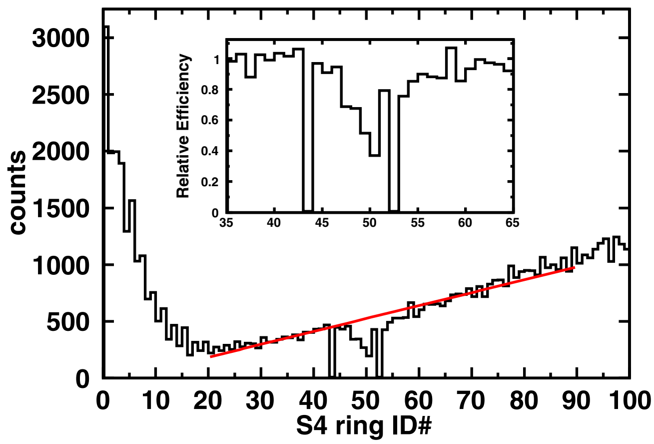

FIG. 6. Distribution of identified protons as a function of S4 ring number. The dip in the distribution from ring numbers 45 to 55 occurs near the location where the inner and outer CsI(Tl) crystals meet. This region also includes the two rings which acquired no usable data. The inset shows the contribution to the efficiency as a function of silicon ring number used in the simulation to incorporate these effects.

Fig. 6). In addition to this, an efficiency loss of ≈5% due to protons undergoing nuclear reactions in the CsI(Tl) crystals was also taken into account [38].

Included in the uncertainty evaluation of the simulated proton efficiency is the reported uncertainty of the proton decay energy of the 2^+ state $E_r = 449(6)$ keV [5]. Starting from a spin 2^+ state and decaying by either a $s_{1/2}$- or $d_{3/2}$-wave proton to the $J=\frac{3}{2}$ residue produces an isotropic emission pattern. We assumed isotropic emission in the simulation. Mixing of the $s_{1/2}$ and $d_{3/2}$ components could lead to some deviation from isotropy but such a deviation could not be discerned.

3. Relative efficiency and beam current

To get the relative detection efficiency for ^{35}K vs ^{36}Ca residues, simulations with relativistic kinematics and the geometry of the setup were performed. The results of the efficiency simulations gave $\varepsilon_{^{35}\mathrm{K}}/\varepsilon_{^{36}\mathrm{Ca}} = 1.03(3)$.

The simulations were set up with a beam-momentum width of ±1% and a radial beam profile that was either Gaussian or uniform in shape. The difference between these simulations is included in the uncertainty estimates. The beam radius was adjusted such that 70% of the beam was transmitted through the ΔE-E ring telescope to the S800, a value matching what was measured. Variation in beam profile and radius only result in a ±1% effect on the value of $\varepsilon_{^{35}\mathrm{K}}/\varepsilon_{^{36}\mathrm{Ca}}$.

Energy-loss calculations were performed for the target and SFA. Efficiency losses through the SFA were assumed to be the same for ^{36}Ca and ^{35}K fragments and thus do not modify the ratio. Transverse and longitudinal momentum distributions after one-neutron knockout of ^{37}Ca to ^{36}Ca(2^+) were calculated with the code MOMDIS [39], assuming 80 : 20 mixing of the $\ell = 0 : 2$ momentum transfers [24]. The longitudinal momentum distributions from MOMDIS, which does not conserve energy, were terminated at the maximum possible value consistent with energy and momentum conservation removing the predicted high-energy tail of this distribution. Variations in the momentum distribution were considered by increasing or decreasing the momentum scale by ±20%. Overall, the details of the momentum distributions have a minor effect on $\varepsilon_{^{35}\mathrm{K}}/\varepsilon_{^{36}\mathrm{Ca}}$ resulting in a ±3% effect on the ratio.

Different rigidity settings of the S800 were used for ^{36}Ca and ^{35}K detection. The S800 nominally has ±3% momentum acceptance in focus mode, but for the detection of ^{36}Ca fragments a blocker was used to reduce the rate of ^{37}Ca at the focal plane in order to increase acquisition live-time. This blocker restricted the S800 high-momentum acceptance further. The high-rigidity cutoff from this blocker was determined from the S800 rigidity spectrum for ^{37}Ca. The location of this cut-off was varied in the simulation to fit the measured distribution. The uncertainty from this fit gives the largest contribution to the uncertainty for $\varepsilon_{^{36}\mathrm{Ca}}$. The final simulated ^{35}K rigidity distribution associated with the 2^+ state matches the experiment quite well.

The number of beam particles was determined by counting light pulses produced in an in-beam scintillator before the target. The total integrated beam was $I_p = 2.02 \times 10^9$ particles during the S800 setting sensitive to ^{35}K and $I_\gamma = 4.05 \times 10^9$ particles during the S800 setting sensitive to ^{36}Ca. A random pulser was used to determine the different acquisition dead times for the two settings. Beam purity was constant throughout the experiment.

TABLE II. Comparison of $B(E2; 0^+ \rightarrow 2_1^+)$ values between experiment and theory. The ZBM2 and USDB results use effective charges of $e_p = 1.36$ and $e_n = 0.45$. The *sdpfu*-mix result [43] uses $e_p = 1.31$ and $e_n = 0.46$.

	$B(E2\uparrow)$ (e^2fm^4)			
	exp	ZBM2 [2]	USDB [42]	*sdpfu*-mix [43]
^{36}Ca	131(20)	179	11.8	23.5
^{36}S	89(9)	116	108	98
^{38}Ca	101(11)	110	14.0	-
^{38}Ar	125(4)	179	128	-

4. Discussion on branching ratio

Using the measured event counts for each decay branch and the simulated efficiencies in Eq. (2) gives a proton branching ratio of $B_p = 0.087(8)$. This value is a small correction to the measured Coulomb-excitation cross section leading to γ-ray emission. Our measured B_p is not in agreement with the value deduced using the ^{37}Ca$(p, d)^{36}$Ca transfer reaction [0.165(10)] [5] but agrees well with the value measured using ^{36}Ca scattering on $^{\mathrm{nat}}$Pb ($0.091^{+0.034}_{-0.019}$) [40].

IV. SHELL-MODEL CALCULATIONS OF $B(E2)$ AND Γ_p

The following discussion considers the $B(E2)$ values reported in this paper and the corresponding mirror nuclei's transition probabilities from Ref. [41]. The experimental and theoretical $B(E2)$ values are given in Table II and are compared in Figs. 7 and 8. The calculated values are from the ZBM2 Hamiltonian in the $(0d_{3/2}, 1s_{1/2}, 0f_{7/2}, 1p_{3/2})$ shell-

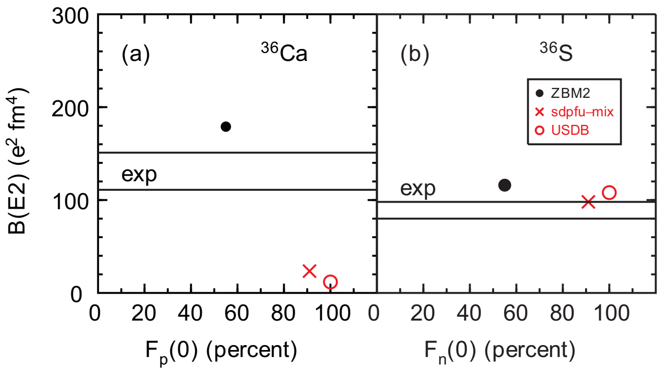

FIG. 7. (a) $B(E2)$ values for ^{36}Ca plotted vs $F_p(0)(^{36}\mathrm{Ca})$. (b) $B(E2)$ values for ^{36}S are plotted vs $F_n(0)(^{36}\mathrm{S})$. As $F_q(0)$ decreases, you increase occupation into the pf shell. The red circles are based on the sd shell calculations with the USDB Hamiltonian [42]. The red crosses are based on the sd-pf calculations from the $sdpfu$-mix interaction [43] with the the $B(E2)$ and F values given in [32]. The black points are from the ZBM2 model space calculations discussed in the text.

model space [2], the USDB Hamiltonian in the sd model space [42], and based on the $sdpfu$-mix plus Coulomb interaction in the sd-pf model space where zero or two protons are allowed to be excited from sd to pf orbitals [43].

The wave functions in the ZBM2 model space can be decomposed into components labeled by $F_q(N_q)$ where F_q is the fraction of the q=proton/neutron part of the wave function that contains N_q protons/neutrons excited from $(0d_{3/2}, 1s_{1/2})$ to $(0f_{7/2}, 1p_{3/2})$. For the sd model space $F_n(0) = F_p(0) = 1$. For the ZBM2 Hamiltonian, the ^{36}Ca ground state has $F_n(0)(^{36}\mathrm{Ca}) = 0.91$, with the largest proton components at $F_p(0)(^{36}\mathrm{Ca}) = 0.55$ and $F_p(2)(^{36}\mathrm{Ca}) = 0.32$. For the sd-pf wave function of [43], the ^{36}Ca ground state has $F_n(0)(^{36}\mathrm{Ca}) = 1$ and $F_p(0)(^{36}\mathrm{Ca}) = 0.92$ [32]. As a result of the ZBM2 model assuming isospin symmetry, the ^{36}S ground state occupations are the same as ^{36}Ca with the protons and neutrons interchanged.

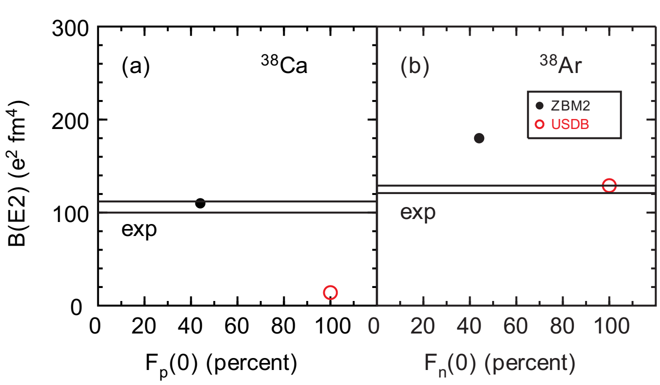

FIG. 8. (a) $B(E2)$ values for ^{38}Ca plotted vs $F_p(0)(^{38}\mathrm{Ca})$. (b) $B(E2)$ values for ^{38}Ar are plotted vs $F_n(0)(^{36}\mathrm{S})$. As $F_q(0)$ decreases, you increase occupation into the pf shell. The red circles are based on the sd shell calculations with the USDB Hamiltonian [42]. The black points are from the ZBM2 model space calculations discussed in the text.

TABLE III. Predicted spectroscopic factors $C^2S_{1/2}$ for the emission of an $s_{1/2}$ proton from the 2^+ state in ^{36}Ca and the corresponding proton partial decay widths calculated with various interactions.

	exp	ZBM2 [2]	sd [42]	sd-pf [43]
$C^2S_{1/2}$	0.0057(10)	0.0056	0.009	0.009
Γ_p	0.53(9)	0.52	0.87	0.84

Figure 7 shows the $B(E2)$ vs $F_p(0)$ correlation for ^{36}Ca and $F_n(0)$ for ^{36}S. Figure 8 shows the same plots for the ^{38}Ca, ^{38}Ar pair. The red circles represent the sd model space in which $F_n(0) = F_p(0) = 1$ is fixed. The red cross present only for ^{36}Ca and ^{36}S are based on the sd-pf calculations from the $sdpfu$-mix interaction where there is a small increase in the pf shell population in the ground state. The black points show the results from the ZBM2 interaction.

The $B(E2)$ values for ^{36}S are not very sensitive to the decreasing fractional occupation of neutrons in the sd shell because $F_p(0)(^{36}\mathrm{S}) \geqslant 0.88$. In contrast, the $B(E2)$ for ^{36}Ca are very sensitive to $F_p(0)(^{36}\mathrm{Ca})$. Modifications to the ZBM2 interaction where the energy gap between the sd and pf shell were artificially increased or decreased gave different fractional occupations. For a small energy gap, the $B(E2)$ shoots up (to about 500 $e^2\mathrm{fm}^4$) while $F_p(0)(^{36}\mathrm{Ca}) = 0$ and $F_p(2)(^{36}\mathrm{Ca})$ dominates the occupation. The opposite is also true where a large energy gap gives a smaller $B(E2)$ (11 $e^2\mathrm{fm}^4$) while $F_p(0)(^{36}\mathrm{Ca}) = 1$.

For ^{36}Ca the experimental $B(E2)$ is a factor of 10 larger than that obtained in the sd model space. With the results shown in Fig. 7, we deduce that the ZBM2 interaction better reproduces the experimental $B(E2)$ values with $F_p(0)(^{36}\mathrm{Ca}) = 0.55(5)$ than the sd model-space result $[F_p(0)(^{36}\mathrm{Ca}) = 1]$, and the sd-pf calculations $[F_p(0)(^{36}\mathrm{Ca}) = 0.92]$ obtained from Refs. [32,43]. This points to ^{36}Ca having increased proton pf-shell occupancy compared to the expected $Z = 20$ closed shell. The results for ^{38}Ca are similar to those for ^{36}Ca. For ^{38}Ca the experimental $B(E2)$ value is a factor of 7 larger than that obtained in the sd model space. This similarly indicates a large pf-shell occupancy in the ground state.

We note that independent of the effective charges assumed, the $B(E2)$ values for the sets $^{36}_{20}\mathrm{Ca}$ and $^{38}_{18}\mathrm{Ar}$ and for $^{38}_{20}\mathrm{Ca}$ and $^{36}_{16}\mathrm{S}$ are similar with the ZBM2 interaction as the calculated $E2$ transition amplitudes for protons and neutrons are similar within these pairs. This similarity of $B(E2)$ values within these pairs is confirmed experimentally (Table II).

From the experimental partial γ decay width and the measured branching ratio, the partial proton decay width of ^{36}Ca is $\Gamma_p = 0.53(9)$ meV. Theoretically this decay width is calculated from the shell-model spectroscopic factor times the single-particle decay width. For the latter we use the same value as in Ref. [5]. Spectroscopic factors for the three shell-model calculations are listed in Table III and resultant partial widths are also given. Of the three shell-model calculations, only the ZBM2 result is consistent with the experimental Γ_p value. Thus the ZBM2 calculation is clearly superior in that it is the only one that reproduces both Γ_γ and Γ_p.

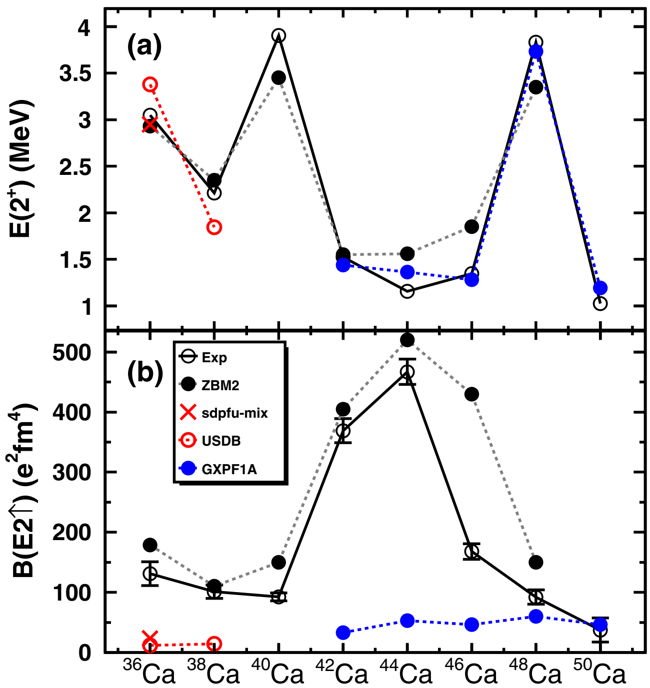

FIG. 9. Comparison of experimental and predicted trends in (a) 2_1^+ excitation energy and (b) $B(E2\uparrow)$ values across the Ca isotopes.

Figure 9 shows trends in both the excitation energies of 2_1^+ states and the $B(E2\uparrow)$ values across the Ca isotopes. The mid-neutron shell around ^{44}Ca shows a sharp increase in $B(E2)$ values from ^{40}Ca while the measured $B(E2)$ values of ^{36,38}Ca are larger than predicted by the *sd* calculations where the trend was expected to dip towards low $B(E2)$ values. Predictions with the ZBM2 interaction give an overall good agreement with both $E(2^+)$ and $B(E2)$ data following the isotopic trends but consistently overpredicts the $B(E2)$. Other shell model interactions, including the GXPF1A (using $e_p = 1.5$ and $e_n = 0.5$) [44], included for $A = 42$–50, have agreement with the $E(2^+)$, but are unable to reconstruct the trend in $B(E2)$ values. The GXPF1A interaction only models neutron occupancy into the *pf* shell and thus results in small $B(E2)$ values. This shows that $B(E2)$ values between neutron closed shells $N = 20, 28$ are sensitive to the degree of $Z = 20$ shell closure and supports the argument for an incomplete $Z = 20$ shell closure. Similarly, the USDB Hamiltonian models neutron occupancy in the *sd* shell and excludes proton excitations resulting in under predicted $B(E2)$ values in ^{36,38}Ca.

The strong occupancy of the *pf* shell is at odds with the recent nuclear density functional calculations of the charge radius of ^{36}Ca [6]. The occupation probability of this shell for the ground state is approximately 13% and as we expect this occupancy is from $(pf)^2$ configurations, then $F_p(0) \approx 0.94$. This value is much closer to the results of the USDB and *sdpfu*-mix shell-model calculations and thus it seems this model would not explain the observed $B(E2)$ value. Clearly more theoretical work is needed to provide a consistent description of the $B(E2)$ strength, the 2^+ proton branching ratio, and the charge radius of ^{36}Ca.

TABLE IV. Evaluated spectroscopic factors from proton removal through the ^{40}Ca$(d,{}^3\mathrm{He})^{39}$K reaction [45] to different levels in ^{39}K compared with predicted spectroscopic factors from the ZBM2 for ^{40}Ca.

E_x (keV)	J^π	ℓ	exp C^2S	ZBM2 C^2S
0	$d_{3/2}$	2	2.20	2.92
2815	$s_{1/2}$	0	1.66	1.48
3020	$f_{7/2}$	3	0.32	0.77
3874	$p_{3/2}$	1	0.05	0.08

It is conceivable that evidence for the high occupancy of the proton *pf* shell could be obtained from proton removal reactions. For ^{40}Ca, measurements of the $(d,{}^3\mathrm{He})$ reaction give spectroscopic factors for the removal of a $\ell = 0, 1, 2, 3$ proton from Ref. [45] which can be compared to the ZBM2 results in Table IV showing it overpredicts the $f_{7/2}$ occupation. The cross section for proton removal from the ^{36}Ca$_{\mathrm{g.s.}}$ to the $3/2^-$ and $7/2^-$ states in ^{35}K would be of interest. Presently only proton and neutron knockout reactions from ^{36}Ca$_{\mathrm{g.s.}}$ to ^{35}K$_{\mathrm{g.s.}}$ and ^{35}Ca$_{\mathrm{g.s.}}$, respectively, have been studied experimentally [46] but the predicted spectroscopic factors for these cases only decrease by 10–20 % with the ZBM2 interaction compared to the *sd* calculations and thus are rather insensitive to the extent of *pf* occupancy.

It is interesting to consider the consequences of the incomplete $Z = 20$ shell closure for the neighboring even-even nucleus ^{34}Ca which has yet to be observed. This nuclide is of interest as it potentially has a bubble structure [47], is possibly a double-magic nucleus [48,49], and is a candidate for a two-proton ground state emitter [50–52]. Most calculations of the nuclear structure and $2p$ decay of ^{34}Ca consider only valence protons in the *sd* shell. With the possibility of both negative and positive parity orbits contributing, then interference effects could lead to a strong diproton configuration for the unbound protons [53–55]. From the ZBM2 Hamiltonian, the two-nucleon amplitudes for removal of two protons from ^{34}Ca$_{\mathrm{g.s.}}$ to ^{32}Ar$_{\mathrm{g.s.}}$ are 0.912 for $(d_{3/2})^2$, 0.313 for $(s_{1/2})^2$, −0.713 for $(f_{7/2})^2$, and −0.224 for $(p_{3/2})^2$.

V. DIFFERENCE IN MIRROR CHARGE RADII UPDATE FOR ^{36}Ca - ^{36}S

In [10] the charge radius of ^{36}Ca was measured, and the difference $\Delta R_{ch} = R_{ch}(^{36}\mathrm{Ca}) - R_{ch}(^{36}\mathrm{S}) = 0.150(4)$ fm was used to deduce a value of of $L =$ 5-70 MeV for the symmetry energy in the nuclear equation of state. The energy-density functional (EDF) and covariant-density functional (CODF) theory calculations that were used for the connection between ΔR and L were based on spherical calculations in the *sd* model space. Deformation corrections to this type of calculation are outlined in [11] where the β_2 parameter of the Bohr model is deduced from the experimental $B(E2)$ value. The ΔR_{ch} for $A = 54$ was then corrected for the changed radii implied by the β_2's.

Using the present results for ^{36}Ca of $B(E2\uparrow) = 131(20)$ e^2fm^4, the deformation correction gives $\beta_2(^{36}\text{Ca}) = 0.139$ and $\delta R_{ch}(^{36}\text{Ca}) = 0.012(2)$ fm. For ^{36}S with the experimental $B(E2) = 89(9)$ e^2 fm^4 [41], we obtain $\beta_2(^{36}\text{S}) = 0.143$ and $\delta R_{ch}(^{36}\text{S}) = 0.013(2)$ fm. Thus one should add $\delta R_{ch}(^{36}\text{Ca}) - \delta R_{ch}(^{36}\text{S}) = -0.001(3)$ fm to the results of the spherical calculations. We conclude that the deformation correction to the $A = 36$ mirror radius difference is small.

The single-particle energies for the pf protons for ^{36}Ca are in the continuum (unbound), but the pf separation energies in the correlated ground-state wave function of ^{36}Ca are positive (e.g., effectively bound). The DFT and CODF calculations used in Ref. [10] assumed a $Z = 20$ closed shell for ^{36}Ca. An extension of the calculations used in Ref. [10] to include the pf orbitals needs to be developed. In Ref. [56], β_2 corrections to the rms radii are not included. Rather, the odd-even oscillations in the rms charge radii are obtained from the addition of a pairing term in the Fayans EDF functional [57]. This leads to a decrease in the correlation between δR_{ch} and L [56].

VI. ^{35}K$(p,\gamma)^{36}$Ca REACTION RATE UPDATE

The astrophysical capture reaction rate through a narrow resonance can be evaluated at the resonance energy E_r to give [58]

$$\langle \sigma v\rangle = \left(\frac{2\pi}{\mu kT}\right)^{3/2} \hbar^2(\omega\gamma)e^{-E_r/kT}, \tag{3}$$

where μ is the reduced mass, kT is the Boltzmann constant times the temperature in Kelvin, and $(\omega\gamma)$ is the resonance strength. The resonance strength for the ^{35}K$(p,\gamma)^{36}$Ca reaction can be expressed in terms of the spins and partial widths Γ_i to give

$$(\omega\gamma) = \frac{2J_i+1}{(2J_p+1)(2J_{35K}+1)}\frac{\Gamma_{\gamma,i}\Gamma_{p,i}}{\Gamma_{\gamma,i}+\Gamma_{p,i}} \tag{4}$$

with the 2^+ state being the resonance of interest, we have $J_i = 2$, $J_p = 1/2$, and $J_{35K} = 3/2$. The energy of this resonance is determined, to high accuracy, to be $E_r = 0.449(6)$ MeV [5]. Only the partial widths make significant contributions to the uncertainty on the reaction rate. The 1^+ and 2_2^+ states in ^{36}Ca, first measured at GANIL [5] and also observed here, can also contribute to the reaction rate but are not significantly populated within the 0.5–2 GK temperature range of an x-ray burst.

TABLE V. Results for the contribution of the first 2^+ state of ^{36}Ca to the ^{35}K$(p,\gamma)^{36}$Ca reaction rate. Results from [5] and the present work are compared.

	GANIL [5]	Present work
B_p	0.165(10)	0.087(8)
$B(E2\downarrow)$ (e^2fm^4)	4.7(2.3)	26.2(40)
Γ_γ (meV)	0.99(45)	5.6(8)
Γ_p (meV)	0.20	0.53(9)
Γ (meV)	1.19(60)	6.1(8)
$(\omega\gamma)$ (meV)	0.10(5)	0.30(7)

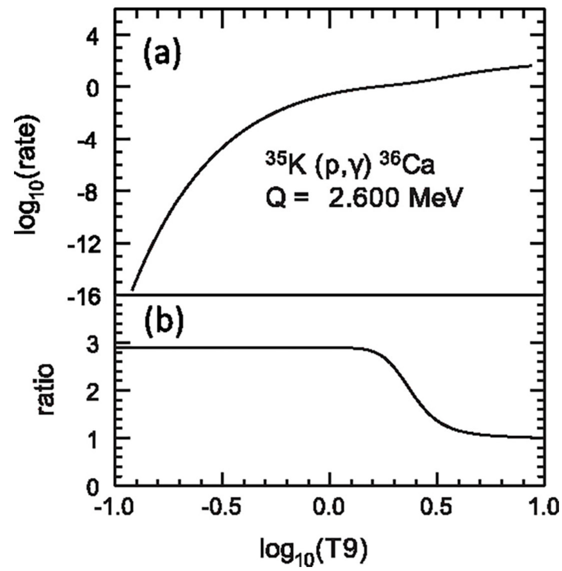

FIG. 10. (a) Present result for the ^{35}K$(p,\gamma)^{36}$Ca reaction rate. (b) Ratio of the present rate divided by the rate obtained in [5].

The reduced transition probability $B(\omega L)$, such as a $B(E2)$ measured here, is directly proportional to the gamma partial width, Γ_γ, as

$$\Gamma_\gamma(\omega L) = \frac{8\pi(L+1)}{L[(2L+1)!!]^2}\left(\frac{E_\gamma}{\hbar c}\right)^{2L+1} B(\omega L). \tag{5}$$

A $B(E2,\ 0_1^+ \to 2_1^+) = 131(20)$ e^2fm^4 or $B(E2,\ 2_1^+ \to 0_1^+) = 26.2(40)$ e^2fm^4 in combination with $E_\gamma = 3.049(3)$ MeV results in $\Gamma_\gamma = 5.6(8)$ meV.

These values are used here in an update to the results by Lalanne [5] which used the *sd-pf* configuration space to calculate $B(E2)$ with an assumed 50% uncertainty and the branching ratio they measured. The parameters relevant for the 2^+ state from the present work and those from the GANIL study are given in Table V. In the present study we measured both the proton decay branch and the $B(E2)$. Our rate is a factor of 3 larger than that of [5] in the astrophysical region (0.5–2 GK) and has a smaller relative uncertainty based entirely on experiment. The details of the input for the new reaction rate are given in Table VI.

The reaction rate is plotted in Fig. 10 along with the ratio of the present rate to the GANIL results. The recommended results of the GANIL study were ≈10% smaller than those of Iliadis *et al.* [59] in the 0.5 to 2 GK range. The latter were used as the default in the sensitivity study of Cyburt *et al.* [12]. In this sensitivity study, increases in the rate by a factor of 100 caused significant modifications in the predicted x-ray burst light curve. Even with our increased rate, we agree with the conclusion of the GANIL study that the ^{35}K$(p,\gamma)^{16}$Ca reaction does not affect the shape of the x-ray bust light curve.

VII. CONCLUSION

The $B(E2,\ 0_1^+ \to 2_1^+)$ values of ^{36}Ca and ^{38}Ca were measured experimentally using the method of intermediate-energy Coulomb excitation to give 131(20) e^2fm^4 and 101(11) e^2fm^4.

TABLE VI. Properties for the relevant rp-resonance states of ^{36}Ca. Only the resonance strength for $J^\pi = 2^+$ is restrained from experiment while the higher energy resonances rely on shell-model calculations with the ZBM2 model [2] for the spectroscopic factors.

n	J^π	k	E_x(th) (MeV)	E_x(exp) (MeV)	E_{res} (MeV)	C^2S $\ell = 0(1)$	C^2S $\ell = 2(3)$	Γ_γ (eV)	Γ_p (eV)	$\omega\gamma$ (eV)
2	2^+	1	3.252	3.049	0.449	5.8×10^{-3}	2.3×10^{-6}	5.6×10^{-3}	5.3×10^{-4}	3.0×10^{-4}
3	1^+	1	5.098	4.270	1.670	2.4×10^{-3}	1.4×10^{-4}	9.5×10^{-2}	7.3×10^{1}	3.5×10^{-2}
4	2^+	2	4.639	4.730	2.130	6.8×10^{-4}	7.4×10^{-3}	3.3×10^{-2}	1.1×10^{2}	2.1×10^{-2}
5	0^+	3	4.924		2.324		6.6×10^{-2}	3.3×10^{-4}	5.4×10^{2}	4.1×10^{-5}
6	4^+	1	5.005		2.405			1.1×10^{-3}		
7	2^+	3	5.378		2.778	5.9×10^{-4}	6.9×10^{-3}	5.9×10^{-3}	3.9×10^{2}	3.7×10^{-3}

The measurement for ^{36}Ca required a correction due to the 2^+ state being unbound to proton decay and the proton branching ratio was measured in a second experiment to be $B_p = 0.087(8)$. The $B(E2)$ value was found to be a factor of 10 larger than predicted by the *sd* shell model and a factor of 5 larger than the *sd*-*pf* shell model which is an indication of a collective excitation.

The present experimental result shows that the ^{36}Ca ground-state wave function contains a significant amount of proton excitation from the *sd* to the *pf* shell. The single-particle energies for the *pf* protons for ^{36}Ca are in the continuum (unbound), but the *pf* separation energies in the correlated ground-state wave function of ^{36}Ca are positive (e.g., effectively bound). Hence, energy density and covariant density functionals containing correlations involving the *pf* orbitals need to be developed.

The measured $B(E2)$ value was used to account for deformation of the nucleus. Because the $B(E2)$ values in the ^{36}Ca/^{36}S mirror pair are similar in value, the correction almost cancels out leaving the difference in charge radii unaffected. This means that the previously reported result for the determination of L from the $A = 36$ stands [10]. Our values for the $B(E2)$ and proton branching ratio have been used to update the ^{35}K$(p,\gamma)^{36}$Ca reaction rate. The rate is increased by a factor of 3 compared to the previous study [5] within the Gamow window of an x-ray burst. While the uncertainties are greatly reduced, the updated rates will not significantly modify the predicted x-ray burst light curves [12].

ACKNOWLEDGMENTS

This material is based upon work supported by the U.S. Department of Energy, Office of Science, Office of Nuclear Physics under Awards No. DE-FG02-87ER-40316 (WU), and DE-SC0020451 (MSU), and Contract No. DE-AC02-06CH11357 (ANL), and by the U.S. National Science Foundation (NSF) under Grants No. PHY-1565546 and No. PHY-2110365, and by the DOE National Nuclear Security Administration through the Nuclear Science and Security Consortium, under Award No. DE-NA0003180. GRETINA was funded by the DOE, Office of Science. Operation of GRETINA at NSCL was supported by the DOE under Grant No. DE-SC0019034.

[1] N. Kitamura, K. Wimmer, A. Poves, N. Shimizu, J. Tostevin, V. Bader, C. Bancroft, D. Barofsky, T. Baugher, D. Bazin, J. Berryman, V. Bildstein, A. Gade, N. Imai, T. Kröll, C. Langer, J. Lloyd, E. Lunderberg, F. Nowacki, G. Perdikakis *et al.*, Phys. Lett. B **822**, 136682 (2021).

[2] E. Caurier, K. Langanke, G. Martínez-Pinedo, F. Nowacki, and P. Vogel, Phys. Lett. B **522**, 240 (2001).

[3] M. L. Bissell, J. Papuga, H. Naïdja, K. Kreim, K. Blaum, M. De Rydt, R. F. Garcia Ruiz, H. Heylen, M. Kowalska, R. Neugart, G. Neyens, W. Nörtershäuser, F. Nowacki, M. M. Rajabali, R. Sanchez, K. Sieja, and D. T. Yordanov, Phys. Rev. Lett. **113**, 052502 (2014).

[4] A. Koszorús, L. Vormawah, R. Beerwerth, M. Bissell, P. Campbell, B. Cheal, C. Devlin, T. Eronen, S. Fritzsche, S. Geldhof, H. Heylen, J. Holt, A. Jokinen, S. Kelly, I. Moore, T. Miyagi, S. Rinta-Antila, A. Voss, and C. Wraith, Phys. Lett. B **819**, 136439 (2021).

[5] L. Lalanne, O. Sorlin, M. Assié, F. Hammache, N. de Séréville, S. Koyama, D. Suzuki, F. Flavigny, D. Beaumel, Y. Blumenfeld, B. A. Brown, F. D. O. Santos, F. Delaunay, S. Franchoo, J. Gibelin, V. Girard-Alcindor, J. Guillot, O. Kamalou, N. Kitamura, V. Lapoux *et al.*, Phys. Rev. C **103**, 055809 (2021).

[6] A. J. Miller, K. Minamisono, A. Klose, D. Garand, C. Kujawa, J. D. Lantis, Y. Liu, B. Maaß, P. F. Mantica, W. Nazarewicz, W. Nörtershäuser, S. V. Pineda, P. G. Reinhard, D. M. Rossi, F. Sommer, C. Sumithrarachchi, A. Teigelhöfer, and J. Watkins, Nat. Phys. **15**, 432 (2019).

[7] T. Glasmacher, Annu. Rev. Nucl. Part. Sci. **48**, 1 (1998).

[8] P. D. Cottle, M. Fauerbach, T. Glasmacher, R. W. Ibbotson, K. W. Kemper, B. Pritychenko, H. Scheit, and M. Steiner, Phys. Rev. C **60**, 031301(R) (1999).

[9] B. A. Brown, Phys. Rev. Lett. **119**, 122502 (2017).

[10] B. A. Brown, K. Minamisono, J. Piekarewicz, H. Hergert, D. Garand, A. Klose, K. König, J. D. Lantis, Y. Liu, B. Maaß, A. J. Miller, W. Nörtershäuser, S. V. Pineda, R. C. Powel, D. M. Rossi, F. Sommer, C. Sumithrarachchi, A. Teigelhöfer, J. Watkins, and R. Wirth, Phys. Rev. Res. **2**, 022035(R) (2020).

[11] S. V. Pineda, K. König, D. M. Rossi, B. A. Brown, A. Incorvati, J. Lantis, K. Minamisono, W. Nörtershäuser, J. Piekarewicz, R. Powel, and F. Sommer, Phys. Rev. Lett. **127**, 182503 (2021).

[12] R. H. Cyburt, A. M. Amthor, A. Heger, E. Johnson, L. Keek, Z. Meisel, H. Schatz, and K. Smith, Astrophys. J. **830**, 55 (2016).

[13] T. Motobayashi, Y. Ikeda, K. Ieki, M. Inoue, N. Iwasa, T. Kikuchi, M. Kurokawa, S. Moriya, S. Ogawa, H. Murakami,

S. Shimoura, Y. Yanagisawa, T. Nakamura, Y. Watanabe, M. Ishihara, T. Teranishi, H. Okuno, and R. Casten, Phys. Lett. B **346**, 9 (1995).
[14] F. Delaunay and F. M. Nunes, J. Phys. G: Nucl. Part. Phys. **34**, 2207 (2007).
[15] J. M. Cook, T. Glasmacher, and A. Gade, Phys. Rev. C **73**, 024315 (2006).
[16] A. Winther and K. Alder, Nucl. Phys. A **319**, 518 (1979).
[17] A. Gade and B. M. Sherrill, Phys. Scr. **91**, 053003 (2016).
[18] D. Morrissey, B. Sherrill, M. Steiner, A. Stolz, and I. Wiedenhoever, Nucl. Instrum. Methods Phys. Res. B **204**, 90 (2003).
[19] D. Bazin, J. Caggiano, B. Sherrill, J. Yurkon, and A. Zeller, Nucl. Instrum. Methods Phys. Res. B **204**, 629 (2003).
[20] S. Paschalis, I. Lee, A. MacChiavelli, C. Campbell, M. Cromaz, S. Gros, J. Pavan, J. Qian, R. Clark, H. Crawford, D. Doering, P. Fallon, C. Lionberger, T. Loew, M. Petri, T. Stezelberger, S. Zimmermann, D. Radford, K. Lagergren, D. Weisshaar *et al.*, Nucl. Instrum. Methods Phys. Res. A **709**, 44 (2013).
[21] D. Weisshaar, D. Bazin, P. Bender, C. Campbell, F. Recchia, V. Bader, T. Baugher, J. Belarge, M. Carpenter, H. Crawford, M. Cromaz, B. Elman, P. Fallon, A. Forney, A. Gade, J. Harker, N. Kobayashi, C. Langer, T. Lauritsen, I. Lee *et al.*, Nucl. Instrum. Methods Phys. Res. A **847**, 187 (2017).
[22] J. Yurkon, D. Bazin, W. Benenson, D. Morrissey, B. Sherrill, D. Swan, and R. Swanson, Nucl. Instrum. Methods Phys. Res. A **422**, 291 (1999).
[23] B. Elman, A. Gade, D. Weisshaar, D. Barofsky, D. Bazin, P. C. Bender, M. Bowry, M. Hjorth-Jensen, K. W. Kemper, S. Lipschutz, E. Lunderberg, N. Sachmpazidi, N. Terpstra, W. B. Walters, A. Westerberg, S. J. Williams, and K. Wimmer, Phys. Rev. C **96**, 044332 (2017).
[24] A. Bürger, F. Azaiez, A. Algora, A. Al-Khatib, B. Bastin, G. Benzoni, R. Borcea, C. Bourgeois, P. Bringel, E. Clément, J.-C. Dalouzy, Z. Dlouhý, Z. Dombrádi, A. Drouart, C. Engelhardt, S. Franchoo, Z. Fülöp, A. Görgen, S. Grévy, H. Hübel *et al.*, Phys. Rev. C **86**, 064609 (2012).
[25] D. Weisshaar, A. Gade, T. Glasmacher, G. F. Grinyer, D. Bazin, P. Adrich, T. Baugher, J. M. Cook, C. A. Diget, S. McDaniel, A. Ratkiewicz, K. P. Siwek, and K. A. Walsh, Nucl. Instrum. Methods Phys. Res. A **624**, 615 (2010).
[26] R. J. Charity, K. W. Brown, J. Elson, W. Reviol, L. G. Sobotka, W. W. Buhro, Z. Chajecki, W. G. Lynch, J. Manfredi, R. Shane, R. H. Showalter, M. B. Tsang, D. Weisshaar, J. Winkelbauer, S. Bedoor, D. G. McNeel, and A. H. Wuosmaa, Phys. Rev. C **99**, 044304 (2019).
[27] L. Riley, D. Weisshaar, H. Crawford, M. Agiorgousis, C. Campbell, M. Cromaz, P. Fallon, A. Gade, S. Gregory, E. Haldeman, L. Jarvis, E. Lawson-John, B. Roberts, B. Sadler, and C. Stine, Nucl. Instrum. Methods Phys. Res. A **1003**, 165305 (2021).
[28] X. Huang and C. Zhou, Nucl. Data Sheets **104**, 283 (2005).
[29] P. Doornenbal, P. Reiter, H. Grawe, T. Otsuka, A. Al-Khatib, A. Banu, T. Beck, F. Becker, P. Bednarczyk, G. Benzoni, A. Bracco, A. Bürger, L. Caceres, F. Camera, S. Chmel, F. C. Crespi, H. Geissel, J. Gerl, M. Górska, J. Grebosz *et al.*, Phys. Lett. B **647**, 237 (2007).
[30] A. Gade, D. Weisshaar, B. A. Brown, D. Bazin, K. W. Brown, R. J. Charity, P. Farris, A. M. Hill, J. Li, B. Longfellow, D. Rhodes, W. Reviol, and J. A. Tostevin, Phys. Rev. C **106**, 064303 (2022).
[31] N. Nica, J. Cameron, and B. Singh, Nucl. Data Sheets **113**, 1 (2012).
[32] L. Lalanne, O. Sorlin, A. Poves, M. Assié, F. Hammache, S. Koyama, D. Suzuki, F. Flavigny, V. Girard-Alcindor, A. Lemasson, A. Matta, T. Roger, D. Beaumel, Y. Blumenfeld, B. A. Brown, F. D. O. Santos, F. Delaunay, N. de Séréville, S. Franchoo, J. Gibelin *et al.*, Phys. Rev. Lett. **129**, 122501 (2022).
[33] P. Endt, At. Data Nucl. Data Tables **55**, 171 (1993).
[34] N. Nica and B. Singh, Nucl. Data Sheets **113**, 1563 (2012).
[35] T. Baugher, Neutron-rich chromium and manganese isotopes and the role of the neutron $0g_{p/2}$ and $1d_{5/2}$ orbitals in the region below ^{68}Ni, Ph.D. thesis, Michigan State University, 2013.
[36] V. Bader, Quadrupole collectivity in neutron-deficient Sn nuclei: ^{104}Sn, Ph.D. thesis, Michgan State University, 2014.
[37] S. Agostinelli, J. Allison, K. Amako, J. Apostolakis, H. Araujo, P. Arce, M. Asai, D. Axen, S. Banerjee, G. Barrand, F. Behner, L. Bellagamba, J. Boudreau, L. Broglia, A. Brunengo, H. Burkhardt, S. Chauvie, J. Chuma, R. Chytracek, G. Cooperman *et al.*, Nucl. Instrum. Methods Phys. Res. A **506**, 250 (2003).
[38] S. Sweany, W. G. Lynch, K. Brown, A. Anthony, Z. Chajecki, D. Dell'Aquila, P. Morfouace, F. C. Teh, C. Y. Tsang, M. B. Tsang, R. S. Wang, and K. Zhu, Nucl. Instrum. Methods Phys. Res. A **1018**, 165798 (2021).
[39] C. A. Bertulani and A. Gade, Comput. Phys. Commun. **175**, 372 (2006).
[40] N. Iwasa, AIP Conf. Proc. **1533**, 159 (2013).
[41] B. Pritychenko, M. Birch, and B. Singh, Nucl. Phys. A **962**, 73 (2017).
[42] B. A. Brown and W. A. Richter, Phys. Rev. C **74**, 034315 (2006).
[43] J. J. Valiente-Dobón, A. Poves, A. Gadea, and B. Fernández-Domínguez, Phys. Rev. C **98**, 011302(R) (2018).
[44] M. Honma, T. Otsuka, B. A. Brown, and T. Mizusaki, Eur. Phys. J. A **25**, 499 (2005).
[45] D. W. Devins, D. L. Friesel, W. P. Jones, A. C. Attard, S. F. Collins, G. G. Shute, B. M. Spicer, V. C. Officer, I. D. Svalbe, R. S. Henderson, and W. E. Dollhopf, Phys. Rev. C **24**, 59 (1981).
[46] R. Shane, R. J. Charity, L. G. Sobotka, D. Bazin, B. A. Brown, A. Gade, G. F. Grinyer, S. McDaniel, A. Ratkiewicz, D. Weisshaar, A. Bonaccorso, and J. A. Tostevin, Phys. Rev. C **85**, 064612 (2012).
[47] G. Saxena, M. Kumawat, M. Kaushik, S. Jain, and M. Aggarwal, Phys. Lett. B **788**, 1 (2019).
[48] A. Poves, J. Phys. G: Nucl. Part. Phys. **44**, 084002 (2017).
[49] G. Saxena, M. Kumawat, M. Kaushik, U. K. Singh, S. K. Jain, S. S. Singh, and Mamta Aggarwal, Int. J. Mod. Phys. E **26**, 1750072 (2017).
[50] L. Grigorenko, I. Mukha, and M. Zhukov, Nucl. Phys. A **714**, 425 (2003).
[51] G. Saxena, M. Kumawat, M. Kaushik, S. Jain, and M. Aggarwal, Phys. Lett. B **775**, 126 (2017).
[52] M. Gonçalves, N. Teruya, O. Tavares, and S. Duarte, Phys. Lett. B **774**, 14 (2017).
[53] Y. Kubota, A. Corsi, G. Authelet, H. Baba, C. Caesar, D. Calvet, A. Delbart, M. Dozono, J. Feng, F. Flavigny, J.-M. Gheller, J. Gibelin, A. Giganon, A. Gillibert, K. Hasegawa, T. Isobe, Y. Kanaya, S. Kawakami, D. Kim, Y. Kikuchi *et al.*, Phys. Rev. Lett. **125**, 252501 (2020).

[54] J. Casal and M. Gómez-Ramos, Phys. Rev. C **104**, 024618 (2021).
[55] T. Oishi, K. Hagino, and H. Sagawa, Phys. Rev. C **82**, 024315 (2010).
[56] P.-G. Reinhard and W. Nazarewicz, Phys. Rev. C **105**, L021301 (2022).
[57] P.-G. Reinhard and W. Nazarewicz, Phys. Rev. C **95**, 064328 (2017).
[58] C. Iliadis, *Nuclear Physics of Stars*, 2nd ed. (Wiley-VCH Verlag GmbH & Co. KGaA, Weinheim, Germany, 2015).
[59] C. Iliadis, R. Longland, A. Champagne, and A. Coc, Nucl. Phys. A **841**, 251 (2010).